DOI 10.1007/s11055-018-0680-7
Neuroscience and Behavioral Physiology, Vol. 48, No. 9, November, 2018

Modeling Light Propagation through the Tissues of the Head Taking Account of Scattering Anisotropy to Optimize the Positioning of Irradiation Detectors and Sources in a Brain–Computer Interface Based on Near Infrared Spectroscopy

M. R. Isaev,[1,2] V. V. Oganesyan,[1,2] D. Husek,[3] and V. Snasel[4]

UDC 612.821

Translated from Zhurnal Vysshei Nervnoi Deyatel'nosti imeni I. P. Pavlova, Vol. 67, No. 4, pp. 546–553, July–August, 2017. Original article submitted April 3, 2017. Accepted May 3, 2017.

We describe here use of the Monte Carlo modeling method to specify the parameters of near infrared light propagation though the tissues of the head, which is needed for optimizing the operation of brain–computer interfaces. The studies used a four-layer spherical model of the head consisting of skin, bone, gray matter, and white matter. The relationship between the parameters of the radiation recorded and the distance between the source and detector were obtained.

Keywords: brain–computer interface, Monte Carlo modeling, near infrared spectrometry, foci of hemodynamic activity.

Introduction. Neurocomputer interfaces have a wide range of uses [Nicolas-Alonso and Gomez-Gil, 2012], mainly in medicine; they have entered use for rehabilitation of poststroke and post-traumatic patients [Frolov et al., 2013; Mokienko et al., 2013; Ivanova et al., 2017]. In the brain–computer interface (BCI) field, use of encephalography is a popular direction [Bobrov et al., 2012]; BCI based on recording the hemodynamic activity of the brain using near infrared spectroscopy (NIRS) is relatively new. NIRS is used in BCI both alone [Power et al., 2012; Strait et al., 2013] and in combination with other methods of recording brain activity [Bobrov et al., 2016; Fazli et al., 2012]. Localization of the sources of this hemodynamic activity and understanding of the nature of the signal recorded promoted creation of more effective interfaces and the development of the field in general. Solution of the inverse problem of determining sources allows NIRS to be used to reconstruct cerebral cortex activity maps. The aims of the present work were to model the passage of near infrared radiation through the tissues of the head and identify the characteristic parameters of this radiation.

NIRS recording of hemodynamic activity is based on the relationship between the level of absorption of infrared radiation passing through brain tissue and the oxy- and deoxyhemoglobin concentrations, which are in turn modulated by brain activity. One recording channel for NIRS signals contains the radiation source and receiver located on the surface of the head. The source sends radiation into brain tissue and the detector records the intensity of light scattered in brain tissues. As scattering and absorption processes are affected by the concentrations of compounds on the irradiation path, changes in the intensity of the detected signal can be used to assess changes in substance concentrations in the tissues, particularly hemodynamic responses.

The passage of radiation was modeled using the Monte Carlo method. This method has been used by various authors in studies of NIRS, to determine or compute parameters and to verify algorithms. Zhang et al. [2012] used the

[1] Pirogov Russian National Research Medical University, Moscow, Russia; e-mail: shycmympuk@yandex.ru.
[2] Moscow Institute of Physics and Technology (State University), Dolgoprudnyi, Moscow Oblast, Russia.
[3] Institute of Informatics, Czech Academy of Sciences, Prague, Czech Republic.
[4] Ostrava Technical University, Ostrava, Czech Republic.

Monte Carlo method to approximate isotropic scattering and a multilayer model of the head to assess the operation of algorithms removing physiological noise in NIRS signals. Selb et al. [2014] used an approximation of isotropic scattering and the same modeling method to compare NIRS and diffusional correlational spectroscopy. The studies of Strangman et al. [2013] and Chuang et al. [2012] should also be noted; both used the Monte Carlo modeling method to determine the optimum NIRS parameters for investigations of the brain.

For the present studies a spherical four-layer model of the head was created, consisting of a skin layer, a bone layer, a gray matter layer, and a white matter layer. The main difference between our study and those listed above was the use of a more realistic anisotropic irradiation model. For each layer, the presence of a particular amount of blood, containing the main absorbers, i.e., oxy- and deoxyhemoglobin, was considered, such that the overall ratio of blood to brain matter in the human brain could be assessed. Propagation of radiation in brain tissues was demonstrated and its parameters were calculated.

Methods. *Monte Carlo modeling*. The distribution of irradiation was modeled using the Monte Carlo method. For each set of initial parameters, one billion photons of wavelength 760 nm were sent down, one after the other, in a direction normal to the surface, from the source located on the top of the head. The propagation of photons through the layers of the head was taken to be anisotropic, and absorption and scattering coefficients were determined, along with substance anisotropy factors, and substance ratios in the layers.

The required coefficients of anisotropic scattering were calculated taking

$$\mu_{aniso} = \mu_{iso}/(1 - g),$$

where μ_{iso} and μ_{aniso} are the coefficients of isotropic and anisotropic scattering.

The length of the mean free path l was calculated for each layer of substance considering the coefficients of absorption μ_a and anisotropic scattering μ_s:

$$l = 1/(\mu_a + \mu_s).$$

A randomly distributed line of path length l_r to the next iteration was calculated at each iteration:

$$l_r = -l^* \log(R),$$

where R is a random value with a uniform distribution between 0 and 1. At the end of the path, the photon is absorbed if

$$R_1 < \mu_a/(\mu_a + \mu_s),$$

where R_1 is also a random value uniformly distributed between 0 and 1, but otherwise is scattered. When scattering occurred, the angles φ and θ were calculated. Angle φ is uniformly distributed between 0 and 2π in the plane perpendicular to the direction of movement of the photon. The scattering angle θ, i.e., the angle between the incident and reflected photon in the plane passing through the neighboring segment of the trajectory was calculated using the Henyey–Greenstein phase function $p(\theta)$ [Pushkareva, 2008], whereby:

$$p(\theta) = \frac{1 - g^2}{(1 + g^2 - 2g\cos\theta)^{3/2}},$$

where g is the anisotropy factor and θ is the scattering angle. In isotropic scattering, angle θ is distributed uniformly between 0 and 2π. If the photon crosses a layer boundary, the iteration finishes at the layer boundary. The iterative process terminates when the photon is detected on the surface of the head.

In view of the cylindrical symmetry of the task, the detector was a ring on the surface of the spherical head with the irradiation source located at the center. Brain activity was modeled in layers with white and gray matter by altering the amount of blood and the blood hemoglobin content. According to Buxton et al. [1998], the local volume of blood in brain tissues increases by 30% on activation, while the oxyhemoglobin content in the veins drops from 80% to 50%, so it can be taken that the mean oxyhemoglobin content in the blood in layers containing white and gray matter drops from 90% to 75%.

Model of head. These studies used a four-layer model of the head (Fig. 1), consisting of four layers: skin, bone, gray matter, and white matter in this order from outside in. The layer boundaries were concentric spheres and their contents were modeled by a substance or a mixture of substances with defined coefficients of absorption and scattering and an anisotropy factor. The first layer (skin) was 4 mm thick with an external radius of 81 mm, an absorption coefficient of 0.18 cm^{-1}, and a coefficient of anisotropic scattering of 119 cm^{-1} [Simpson et al., 1998]. Jacques [1996] indicated that the relationship between the anisotropy factor of the skin and photon wavelength was described by the following empirical equation:

$$g(\lambda) = 0.7645 + 0.2355\{1 - \exp[(-\lambda - 500\ \text{nm})/729.1\ \text{nm}]\},$$

where λ is wavelength. At a photon wavelength 760 nm, the anisotropy factor of the skin layer was taken as 0.84 [Pushkareva, 2008]. Because of the low content of blood in human skin [Jacques, 2013], the quantity in this layer was taken as 0. The second layer, bone, was 7 mm thick with an external radius of 77 mm, a coefficient of absorption of 0.16 cm^{-1} [Fukui et al., 2003], a coefficient of anisotropic scattering of 229 cm^{-1} [Firbank et al., 1993; Fukui et al., 2003], and an anisotropy factor of 0.93 [Firbank et al., 1993]. For the same reasons as for skin, the quantity of blood in the bone layer was taken as 0. Working from the ratio of the volume of blood in the brain to the quantity of brain matter [Rengachary and Ellenbogen, 2005], the ratio

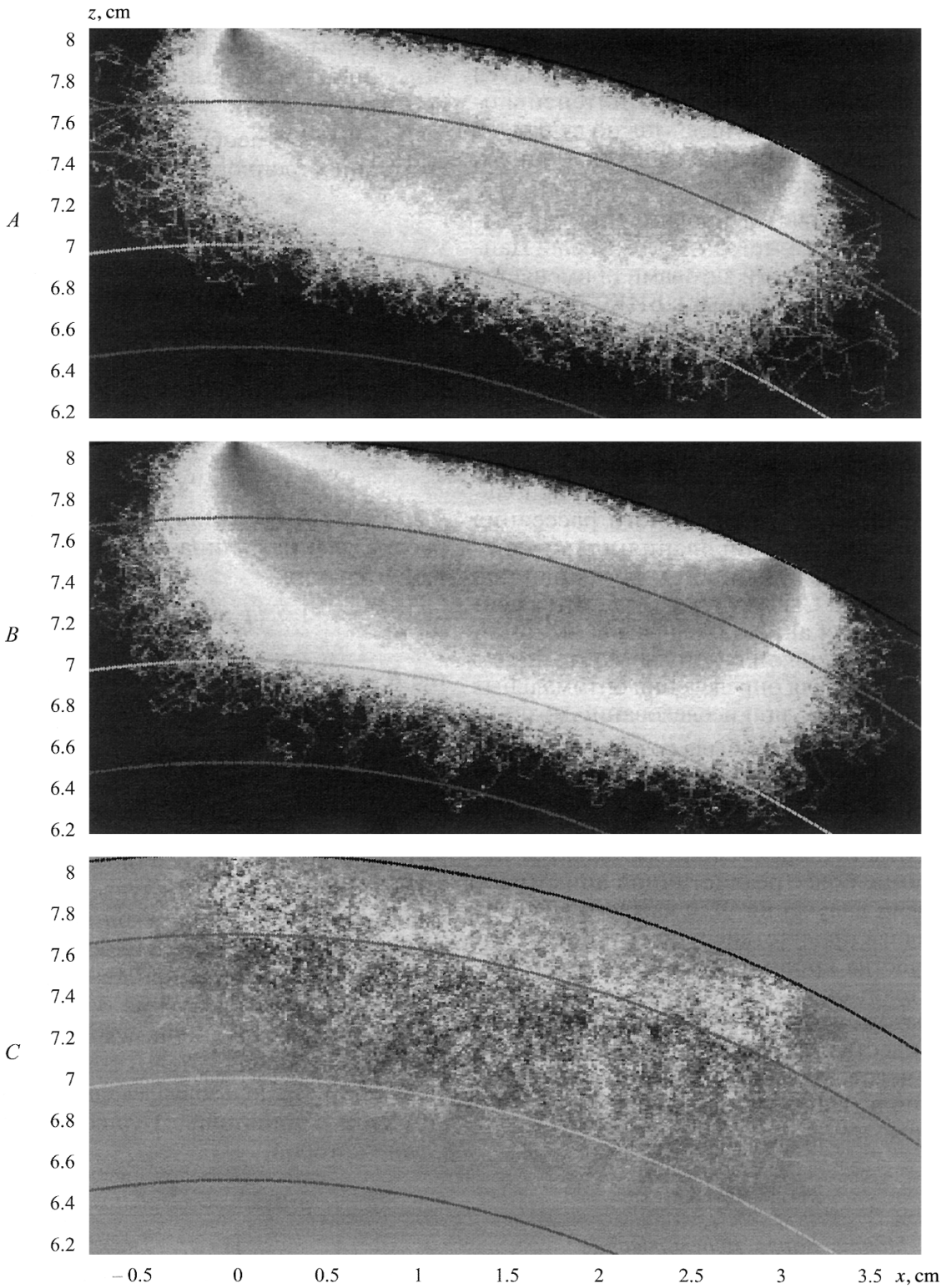

Fig. 1. Main pathway of the propagation of irradiation from source to detector. Changes in color from dark to light correspond to decreases in the probability that the photon will pass through a given region. *A*) isotropic scattering; *B*) anisotropic scattering; *C*) difference between *A* and *B*.

of the cerebral blood volume in the white and gray matter [Le et al., 2006], and also the ratio of the quantity of white and gray matter in the brain [Good et al., 2003], the volumes of blood in the white and gray matter layers were calculated.

The third layer, 5 mm thick, was modeled as a mixture of gray matter with a coefficient of absorption of 0.3 cm^{-1}, a coefficient of anisotropic scattering of 650 cm^{-1}, and an anisotropy factor of 0.96 [Vander Zee et al., 1993] and blood

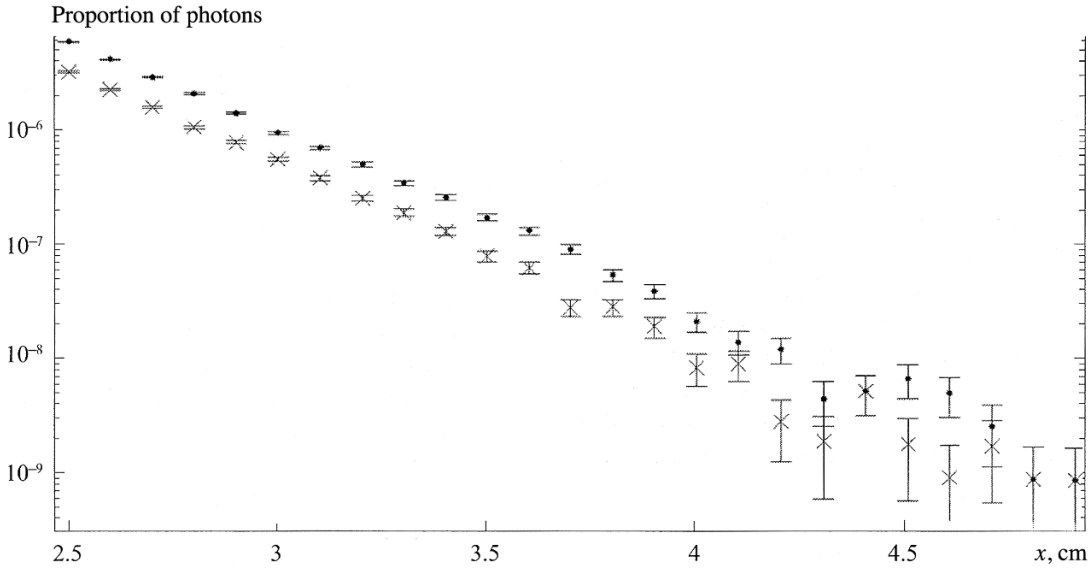

Fig. 2. Relationship between the proportion of photons recorded and the distance between the irradiation source and detector. The plot shows mean values and errors of the mean: ×) isotropic scattering; •) anisotropic scattering.

at a ratio of 7.72:1. The external radius of this layer was taken as 70 mm. The fourth layer, with an external radius of 65 mm, was a mixture of white matter and blood at a ratio of 15.43:1. The coefficients of absorption and anisotropic scattering and the anisotropy factor of white matter without considering blood were taken as 0.1 cm^{-1}, 500 cm^{-1}, and 0.82, respectively [Vander Zee et al., 1993].

The optical properties of the blood, depending on the irradiation wavelength, according to [Douven and Lucassen, 2000], can be described as follows:

$$\mu_a^{blood}(\lambda) = p^{Oxy}\mu_a^{HbO_2}(\lambda) + (1 - p^{Oxy})\mu_a^{Hb}(\lambda);$$

$$\mu_s^{blood}(\lambda) = 440.72H(1-H)\frac{685}{\lambda};$$

$$g^{blood}(\lambda) = 0.995,$$

where λ is the photon wavelength in nm, $\mu_a^{blood}(\lambda)$ and $\mu_s^{blood}(\lambda)$ are the coefficients of absorption and anisotropic scattering, respectively, and p^{Oxy} is the blood oxygen saturation (for example, $p^{Oxy} = 0.8$ means that the blood contains 80% oxyhemoglobin (HbO_2) and 20% deoxyhemoglobin, $\mu_a^{HB}(\lambda)$ and $\mu_a^{HbO_2}$ are the coefficients of absorption of hemoglobin and oxyhemoglobin, respectively, H is the hematocrit, and $g^{blood}(\lambda)$ is the anisotropy factor. For the wavelength of 760 nm used here, $H = 0.44$, $\mu_a^{HbO_2} = 1486$ liters·cm^{-1}·mol^{-1}, $\mu_a^{Hb} = 3843$ liters·cm^{-1}·mol^{-1}, $p^{Oxy} = 0.9$, and blood hemoglobin concentration = 150 g/liter, which gave the following coefficients of absorption and anisotropic scattering: 3.87 cm^{-1} and 940 cm^{-1}, respectively.

Results. Figure 1 shows the main path for propagation of irradiation from the source through the tissues of the head to the detector located 3 cm from the source and 2 mm in diameter. Changes in color from dark to light correspond to decreases in the probability of a photon passing though this region. A is isotropic scattering and B is anisotropic scattering; C is the difference between A and B.

Selecting a different distance from the irradiation source to the detector in the model provides the relationship between the proportion of photons recorded and distance. This relationship is shown in Fig. 2 on a log scale. Dots and crosses show the anisotropic and isotropic models, respectively. The detectors, of size 1 mm, were located 1 mm from each other.

The relationship between the ratio of the number of photons passing through the layer containing gray matter on their route to the detector to the number of photons reaching a given detector and distance was obtained in a similar way. This relationship is presented in Fig. 3, where dots show the anisotropic model and crosses show the isotropic model. Detector size and the distance between them were 1 mm.

The proportion of photons reaching all detectors located 2.5 cm or more from the source in the isotropic and anisotropic cases were $(1072 \pm 10)\cdot 10^{-8}$ and $(2058 \pm 14)\cdot 10^{-8}$, respectively. The ratio of the number of photons whose path to the detector passed through the layer containing gray matter to the number of photons reaching a given detector for the isotropic and anisotropic approximations were 0.199 ± 0.006 and 0.270 ± 0.006, respectively. These values for the isotropic and anisotropic cases differed by 92% and 36%, respectively. Because of such large differences, further results are given only for anisotropic scattering.

Brain activity in these areas of the gray and white matter was modeled in terms of changes in the volume content of blood in the different layers and the ratio of oxy- to deoxyhemoglobin. Wen activity was specified throughout the

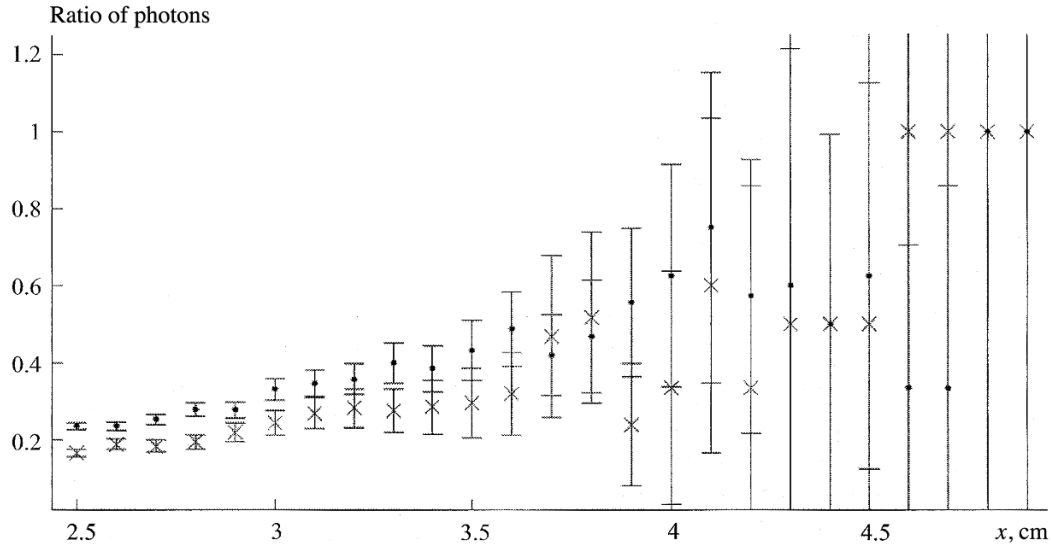

Fig. 3. Relationship between the distance between the source and detector and the ratio of the number of photons which pass through the layer containing the gray matter on their path to the detector to the number of photons reaching this detector. The plot shows mean values and errors of the mean: ×) isotropic scattering; •) anisotropic scattering.

gray and white matter, the proportion of photons reaching all the detectors 2.5 cm or more from the source decreased significantly, from $(2058 \pm 14)\cdot 10^{-8}$ to $(1939 \pm 14)\cdot 10^{-8}$ ($p < 0.05$). Thus, a change in blood filling by 30% throughout the volume of the gray and white matter, along with a change in the proportion of oxyhemoglobin in venous blood from 0.8 to 0.5, led to decreases in the intensity of the recorded signal by 6%. A cylinder of radius 1.5 cm was then selected as the area of activity in the gray and white matter, the axis of the cylinder coinciding with the direction of the path of photons from the source. In this situation, the proportion of passing photons decreased slightly, to $(1998 \pm \pm 14)\cdot 10^{-8}$ ($0.05 < p < 0.1$), while in the case of an area equal to the entire gray and white matter, apart from the cylinder, it decreased to $(1994 \pm 14)\cdot 10^{-8}$ ($0.05 < p < 0.1$).

Discussion. The shape found for the main trajectories for the propagation of light in the tissues of the head were consistent with published results. In fact, the main path for irradiation in this model passes through the layers representing the skin and bony tissue and, thus, changes in the optical parameters of these layers during data recording have significant influences on the result obtained. Thus, there is a need to take measures to eliminate, weaken, or account for this influence in studies of brain activity using NIRS. It is also of note that the projection of the study area of the brain onto the surface of the head must be located between the irradiation source and detector, so this is where the main paths of photons reaching the layer containing gray matter project. At a distance of 3 cm between optodes, this area is a region modeling the cerebral cortex.

The relationship obtained between the proportion of photons reaching the detector and the distance between the irradiation source and the detector led to a number of conclusions regarding the optimum positioning of the optodes on the head surface. As expected from the Bouguer–Beer–Lambert law, there was an exponential drop in the intensity of the recorded irradiation with linear increases in the distance between the source and the detector. Thus, in the case of using NIRS in BCI, unremovable equipment noise will block the useful signal starting from some particular value of this distance.

On the other hand, as seen from the relationship between the proportion of photons passing through the third layer, decreases in the distance between optodes have the result that a smaller proportion of radiation reaches the modeled cerebral cortex, so changes in the optical properties of the upper layers, modeling skin and bone, such as oscillations associated with physiological changes in these layers, start to make a significant contribution to the recorded signal.

Thus, the optimum distance between the source and the detector lies in some range limited above and below by the effects of equipment and physiological factors. And study, assessment, and removal of the influences of these noises on the resulting signal are required to improve the operation of brain–computer interfaces based on NIRS.

Modeling of the influences of brain activity on the optical properties of the medium in terms of changes in the composition and quantity of blood in the white and gray matter layers allows us to understand that the size and position of the focus of hemodynamic activity influence the proportion of photons reaching the detector. Increases in the statistical significance of modeling and consideration of this influence provide for increases in the accuracy of solutions to the inverse task of seeking sources of activity using NIRS.

Conclusions

1. The projection of the of the brain studied by NIRS onto the surface of the head is located between the irradiation receiver and the source.

2. The proportion of photons detected decreases exponentially as the distance between the source and the detector increases linearly.

3. As the distance between the signal source and receiver increases, areas containing white and gray matter make increasing contributions to the signal recorded.

4. Changes in blood filling by 30% throughout the volume of the gray and white matter, along with changes in the proportion of oxyhemoglobin in venous blood from 0.8 to 0.5, which corresponds to physiologically sensible changes in these parameters, lead to a 6% decrease in the intensity of the signal recorded.

This study was supported by the Russian Federation Ministry of Education and Science (Grant No. RFMEFI 60715X0128).

REFERENCES

Bobrov, P. D., Korshakov, A. V., Roshchin, V. Yu., and Frolov, A. A., "A Bayesian approach to brain–computer interfaces based on motor imagery," *Zh. Vyssh. Nerv. Deyat. I. P. Pavlova*, **62**, No. 1, 1–11 (2012).

Bobrov, P. D., Isaev, M. R., Korshakov, A. V., Oganesyan, V. V., Kerechanin, Ya. V., Popod'ko, A. I., and Frolov, A. A., "Sources of electrophysiological and foci of hemodynamic activity in the brain significant for the control of a hybrid brain–computer interface based on the recognition of EEG patterns and near infrared spectrograms on motor imagery," *Fiziol. Cheloveka*, **42**, No. 3, 12–24 (2016).

Ivanova, G. E., Bushkova, Yu. V., Suvorov, A. Yu., Stakhovskaya, I. Z., Dzhalagoniya, I. Z., Varako, N. A., Kovyazina, M. S., and Bushkov, F. A., "Use of 'BCI-exoskeleton' simulators with multichannel biological feedback in complex rehabilitation programs in poststroke patients," *Zh. Vyssh. Nerv. Deyat. I. P. Pavlova*, **67**, No. 4, 464–472 (2017).

Mokienko, O. A., Bobrov, P. D., Chernikova, L. A., and Frolov, A. A., "Motor imagery-based brain–computer interface in the rehabilitation of patients with hemiparesis," *Byull. Sibirsk. Med.*, **12**, No. 2, 30–35 (2013).

Pushkareva, A. E., *Methods for Mathematical Modeling in Biotissue Optics*, St. Petersburg State University of Information Technologies, Mechanics, and Optics (2008).

Frolov, A. A., Biryukova, E. V., Bobrov, L. D., Mokienko, O. A., Platonov, A. K., Pryanichnikov, V. E., and Chernikova, L. A., "Principles of neurorehabilitation based on use of 'brain–computer interfaces' and biologically appropriate control of an exoskeleton," *Fiziol. Cheloveka*, **39**, No. 2, 99–113 (2013).

Buxton, R. B., Wong, E. C., and Frank, L. R., "Dynamics of blood flow and oxygenation changes during brain activation: the balloon model," *Magn. Reson. Med.*, **39**, No. 6, 855–864 (1998).

Chuang, C. C., Lee, Y. T., Chen, C. M., Hsieh, Y. S., Liu, T. C., and Sun, C. W., "Patient-oriented simulation based on Monte Carlo algorithm by using MRI data," *Biomed. Eng. Online*, **11**, No. 1, 11–21 (2012).

Douven, L. F. A. and Lucassen, G. W., "Retrieval of optical properties of skin from measurement and modeling the diffuse reflectance," in: Bi*OS 2000. The International Symposium on Biomedical Optics*, International Society for Optics and Photonics (2000), pp. 312–323.

Fazli, S., Mehnert, J., Steinbrink, J., Curio, G., Villringer, A., Müller, K. R., and Blankertz, B., "Enhanced performance by a hybrid NIRS–EEG brain computer interface," *Neuroimage*, **59**, No. 1, 519–529 (2012).

Firbank, M., Hiraoka, M., Essenpreis, M., and Delpy, D. T., "Measurement of the optical properties of the skull in the wavelength range 650–950 nm," *Phys. Med. Biol.*, **38**, No. 4, 503–510 (1993).

Fukui, Y., Ajichi, Y., and Okada, E., "Monte Carlo prediction of near infrared light propagation in realistic adult and neonatal head models," *Applied Optics*, **42**, No. 16, 2881–2887 (2003).

Good, C. D., Johnsrude, I. S., Ashburner, J., Ilenson, R. N., Friston, K. J., and Frackowiak, R. S., "A voxel-based morphometric study of ageing in 465 normal adult human brains," *Neuroimage*, **14**, 21–36 (2001).

Jacques, S. L., "Optical properties of biological tissues: a review," *Phys. Med. Biol.*, **58**, No. 11, R37–R61 (2013).

Jacques, S. L., "Origins of tissue optical properties in the UVA, visible, and NIR regions," *OSA TOPS on Advances in Optical Imaging and Photon Migration*, No. 2, 364–369 (1996).

Lee, M. C., Cha, S., Chang, S. M., and Nelson, S. J., "Partial-volume model for determining white matter and gray matter cerebral blood volume for analysis of gliomas," *J. Magn. Reson. Imaging*, **23**, No. 3, 257–266 (2006).

Nicolas-Alonso, L. F. and Gomez-Gil, J., "Brain computer interfaces, a review," *Sensors*, **12**, No. 2, 1211–1279 (2012).

Power, S. D., Kushki, A., and Chau, T., "Automatic single-trial discrimination of mental arithmetic, mental singing and the nocontrol state from prefrontal activity: toward a three-state NIRS-BCI," *BMC Res. Notes*, **5**, No. 1, 1–10 (2012).

Rengachary, S. S. and Ellenbogen, R. G. (eds.), *Principles of Neurosurgery*, Elsevier Mosby (2005).

Selb, J., Boas, D. A., Chan, S. T., Evans, K. C., Buckley, E. M., and Carp, S. A., "Sensitivity of near-infrared spectroscopy and diffuse correlation spectroscopy to brain hemodynamics: simulations and experimental findings during hypercapnia," *Neurophotonics*, **1**, No. 1, 015005–015005 (2014).

Simpson, C. R., Kohl, M., Essenpreis, M., and Cope, M., "Near-infrared optical properties of ex vivo human skin and subcutaneous tissues measured using the Monte Carlo inversion technique," *Phys. Med. Biol.*, **43**, No. 9, 2465–2478 (1998).

Strait, M., Canning, C., and Scheutz, M., "Limitations of NIRS-based BCI for realistic applications in human-computer interaction," in: *Proceedings of the Fifth International Brain–Computer Interface Meeting* (2013), Article 2.

Strangman, G. E., Li, Z., and Zhang, Q., "Depth sensitivity and source-detector separations for near infrared spectroscopy based on the Colin27 brain template," *PLoS One*, **8**, No. 8, e66319 (2013).

Van der Zee, P., Essenpreis, M., and Delpy, D. T., "Optical properties of brain tissue," in: *OE/LASE'93: Optics, Electro-Optics, & Laser Applications in Science & Engineering*, International Society for Optics and Photonics (1993), pp. 454–465.

Zhang, Y., Sun, J. W., and Rolfe, P., "RLS adaptive filtering for physiological interference reduction in NIRS brain activity measurement: a Monte Carlo study," *Physiol. Meas.*, **33**, No. 6, 925–942 (2012).